

Bifurcations, time-series analysis of observables, and network properties in a tripartite quantum system

Pradip Laha,* S. Lakshmibala, and V. Balakrishnan
Department of Physics, IIT Madras, Chennai 600036, India

(Dated: May 22, 2020)

In a tripartite system comprising a Λ -atom interacting with two radiation fields in the presence of field nonlinearities and an intensity-dependent field-atom coupling, striking features have been shown to occur in the dynamics of the mean photon number $\langle N_i(t) \rangle$ ($i = 1, 2$) corresponding to either field. In this Letter, we carry out a detailed time-series analysis and establish an interesting correlation between the short-time and long-time dynamics of $\langle N_i(t) \rangle$. Lyapunov exponents, return maps, recurrence plots, recurrence-time statistics, as well as the clustering coefficient and the transitivity of networks constructed from the time series, are studied as functions of the intensity parameter κ . These are shown to carry signatures of a special value $\kappa = \bar{\kappa}$. Our work also exhibits how techniques from nonlinear dynamics help analyze the behavior of observables in multipartite quantum systems.

PACS numbers: 05.45.Tp; 42.50.-p; 05.45.-a

I. INTRODUCTION

In machine-learning protocols and in solutions to problems involving computationally intensive procedures, reduction of a large data set to a considerably smaller optimal set [1] poses a challenge. Network analysis provides an effective solution to this problem, particularly in the context of machine learning [1, 2]. Further, long time series of classical dynamical variables need to be investigated in a variety of contexts ranging from weather forecasting and climate analysis to medical research [3–7]. The tools of network analysis have been used in these examples to select an optimal subset of data points in the time series for investigating the underlying dynamics. Different indicators that capture the important features of the time series have been identified from such smaller data sets in model classical systems [8].

In the quantum context, too, large data sets pertaining to the dynamics of appropriate observables have been either measured in specific experiments, or obtained through numerical simulations in certain cases (see, e.g., [9]). Quantum optics provides a wide range of experimentally realizable examples in which both the short-time behavior and the long-time behavior exhibit interesting dynamical properties. The diversity of the ergodicity properties displayed by experimentally measurable quantum mechanical expectation values provides the motivation to employ the tools of time-series analysis such as first-return-time distributions, recurrence plots, calculation of Lyapunov exponents, and so on, to understand the temporal behavior of these observables. In the case of the bipartite model considered in Ref. [10], investigations along these lines have been carried out in earlier work [11, 12]. This model describes a multilevel atom of a nonlinear medium interacting with a radiation field. For sufficiently high nonlinearity (relative to the

interaction strength), it has been shown that the dynamics of the mean photon number can exhibit exponential instability, as indicated by a positive maximal Lyapunov exponent (MLE). In the case of a multipartite model of a three-level Λ -atom interacting with either one or two radiation fields, a detailed time-series analysis [13] of the mean photon number of either field, $\langle N_i(t) \rangle$ ($i = 1, 2$), reveals a wide range of ergodic behavior, depending sensitively on the strength of the nonlinearity and the degree of coherence of the initial state of the radiation field(s).

Another aspect of the dynamics of quantum observables pertains to the nonclassical effects that are manifested in the time series. These effects include quadrature and entropic squeezing [14–16], sudden death of the entanglement between subsystems [17], and the collapse of the entanglement to a constant non-zero value over a significant time-interval [15, 18]. This entanglement collapse is highly sensitive to the initial state considered and the field nonlinearities. In particular, in the tripartite model mentioned above, the entanglement of the atomic subsystem collapses to a fixed non-zero value over a significant time interval [18]. This is also reflected in the dynamics of both the mean and the variance of the photon number corresponding to either of the two field modes.

Apart from field nonlinearities, several experimental techniques have been developed in recent years to create nonlinear interactions between photons and single atoms (see, for instance, [19]). The rather simple procedure of coupling light to a single atom by focusing the incident photons onto the atom with a lens only provides moderate interaction strengths. This hurdle has been overcome recently by adapting a super-resolution imaging technique, namely, 4Pi microscopy. A test of the nonlinear interaction is the experimental observation of modified photon statistics of the transmitted field [19].

If the field-atom coupling in the above model describing a Λ -atom interacting with light [18] is dependent on the field intensity, new phenomena occur. Several forms of intensity-dependent couplings (IDCs) have been intro-

* pradip@physics.iitm.ac.in

duced and analyzed in the literature to understand the dynamical behavior of the system. Some of them are: $f(N_i) = N_i^{1/2}$ [20], $N_i^{-1/2}$ [21], $(1 + \kappa N_i)^{1/2}$ [22] and $(1 - \frac{1}{2}\eta^2 N_i)$ [23]. Here κ is the ‘intensity parameter’ and η is another such parameter (the Lamb-Dicke parameter). In particular, for an intensity-dependent coupling of the form $f(N_i) = (1 + \kappa N_i)^{1/2}$, the mean photon number $\langle N_i \rangle$ exhibits an interesting bifurcation cascade as κ is varied from 0 to 1 [18]. Significantly, there is an underlying algebra of field operators associated with this particular functional form of the coupling. Let $R = a f(N)$ and $R_0 = \frac{1}{2} + \kappa(N + \frac{1}{2})$ where $N = a^\dagger a$ (a and a^\dagger are the photon annihilation and creation operators, respectively) and $f(N) = (1 + \kappa N)^{1/2}$. Then the operators R, R^\dagger and R_0 satisfy a closed algebra under commutation:

$$[R, R^\dagger] = 2R_0, \quad [R, R_0] = \kappa R, \quad [R^\dagger, R_0] = -\kappa R^\dagger. \quad (1)$$

This is a deformation of the Lie algebra corresponding to the group $SU(1,1)$, with κ as the deformation parameter. The limiting case $\kappa = 0$ reduces to the usual Heisenberg-Weyl algebra for the field operators, while the case $\kappa = 1$ yields the Lie algebra of the group $SU(1, 1)$. Hence, by varying κ from 0 to 1, we can examine the effects of a continuous change in the algebra of the operators relevant to the system on the dynamics (specifically, on the ergodic properties of a suitable dynamical variable), although this precise form of the IDC has not been realized experimentally as yet. It has also been verified that, for the IDCs $f(N_i) = N_i^{1/2}$ and $N_i^{-1/2}$, the dynamics is not as rich as it is for $f(N_i) = (1 + \kappa N_i)^{1/2}$ [18]. The possibility of experimentally exploring the consequences of the specific form $f(N_i) = (1 - \frac{1}{2}\eta^2 N_i)$ has been examined [23], although in the system under consideration this IDC does not lead to the diverse dynamical effects displayed when $f(N_i) = (1 + \kappa N_i)^{1/2}$. For all the reasons described in the foregoing, we focus on the latter choice of IDC in what follows.

Recently, an ϵ -recurrence network has been constructed [24] for the time series of $\langle N_i(t) \rangle$. It has been shown that the signatures of the bifurcation cascade are also captured in the manner in which the clustering coefficient and the transitivity of the network vary with κ . In the light of this fact, certain significant questions arise: do these network quantifiers reflect the properties of the cascade if the ϵ -recurrence network is replaced by other types of networks? Do network quantifiers such as the transitivity, clustering coefficients, etc., also exhibit interesting features deduced from the MLEs, return maps, recurrence plots and recurrence-time distributions? In particular, is there a relation between the manner in which these important elements in the theory of dynamical systems (on the one hand) and network properties (on the other) vary with changes in the relevant parameters of the system (in this case, κ)? The purpose of this Letter is to address these questions.

The relevant features of the tripartite model considered are given in Sec. II. In Sec. III, we present a brief review

of the manner in which the properties of the network correlate with the bifurcation sequence exhibited by $\langle N_i \rangle$. Section IV is devoted to the MLEs, return maps, recurrence plots and first-return-time distributions for different values of κ . The occurrence and effect of a special value $\bar{\kappa}$ on the network properties such as the clustering coefficients and the transitivity are also discussed. The inferences to be drawn from this work are summed up in Sec. V. The key steps in the derivation of the state of the system at any time t are outlined in the Appendix.

II. THE TRIPARTITE MODEL

We consider a Λ -atom inside a cavity, interacting with a probe field F_1 and a coupling field F_2 with respective frequencies Ω_1 and Ω_2 (see, e.g., Fig. 1 of Ref. [24]). The corresponding photon annihilation and creation operators are a_i and a_i^\dagger , ($i = 1, 2$). The two lower energy states of the Λ -atom are denoted by $|1\rangle$ and $|2\rangle$, respectively, and the excited state by $|3\rangle$. The fields F_1 and F_2 induce $|1\rangle \leftrightarrow |3\rangle$ and $|2\rangle \leftrightarrow |3\rangle$ transitions, respectively. The transition $|1\rangle \leftrightarrow |2\rangle$ is dipole-forbidden. The Hamiltonian incorporating field nonlinearities and field-atom IDC is given (with $\hbar = 1$) by

$$H = \sum_{j=1}^3 \omega_j \sigma_{jj} + \sum_{i=1}^2 \left\{ \Omega_i a_i^\dagger a_i + \chi a_i^{\dagger 2} a_i^2 + \lambda [a_i f(N_i) \sigma_{3i} + f(N_i) a_i^\dagger \sigma_{i3}] \right\}. \quad (2)$$

Here, $\sigma_{jk} \equiv |j\rangle \langle k|$ are the Pauli spin operators (where $|j\rangle$ denotes an atomic state), and ω_j are positive constants. χ is the strength of the nonlinearity in both the fields, and λ is the atom-field coupling parameter. As mentioned earlier, the IDC $f(N_i) = (1 + \kappa_i N_i)^{1/2}$ with $N_i = a_i^\dagger a_i$. For simplicity, in our calculations we set the detuning parameter to zero, i.e., $\omega_3 - \omega_i - \Omega_i = 0$ ($i = 1, 2$), and also set $\kappa_2 = 0$ and $\kappa_1 = \kappa$ where $0 \leq \kappa \leq 1$.

The D_1 transition in an ^{85}Rb atom driven by a pump and a coupling field is an example of a Λ -atom interacting with two radiation fields. In this system, the two ground states of the atom correspond to the hyperfine levels $5S_{1/2}$ ($F = 2$) and $5S_{1/2}$ ($F = 3$), while the excited state corresponds to the $5P_{1/2}$ in the D_1 line of the ^{85}Rb atom. In a sense this is the ‘workhorse’ of quantum optics. Several new phenomena including electromagnetically induced transparency (or absorption) have been investigated extensively, both experimentally and theoretically, in this system (for further details see, for instance, [25–28]).

The field nonlinearity in our model is Kerr-like, i.e., of the form $a_i^{\dagger 2} a_i^2$ (see Eq.(2)). This type of nonlinearity has been used in several theoretical models and is readily realizable experimentally. Exhaustive work on Kerr nonlinearities has been reported in the literature. Some recent interesting results may be found in [29–31].

We take the initial states of both the fields to be the standard normalized coherent state (CS)

$$|\alpha\rangle = \sum_{n=0}^{\infty} q_n(\alpha) |n\rangle, \quad q_n(\alpha) = \frac{e^{-|\alpha|^2/2} \alpha^n}{\sqrt{n!}}, \quad (3)$$

where $\alpha \in \mathbb{C}$, and that of the atom to be the state $|1\rangle$. Hence the initial state of the system is given by

$$|\psi(0)\rangle = \sum_{n=0}^{\infty} \sum_{m=0}^{\infty} q_n(\alpha) q_m(\alpha) |1; n; m\rangle, \quad (4)$$

where the labels in the ket vector refer respectively to the state of the atom and the number states of the two fields. Solving the Schrödinger equation in the interaction picture, the state of the system at any time $t > 0$ is found to be of the form

$$|\psi(t)\rangle = \sum_{n=0}^{\infty} \sum_{m=0}^{\infty} q_n(\alpha) q_m(\alpha) \left\{ A_{nm}(t) |1; n; m\rangle + B_{nm}(t) |2; n-1; m+1\rangle + C_{nm}(t) |3; n-1; m\rangle \right\}. \quad (5)$$

Explicit expressions are given in the Appendix for the time-dependent coefficients A_{nm} , B_{nm} , C_{nm} , and for the reduced density matrices of the subsystems.

III. BIFURCATION CASCADE AND NETWORK ANALYSIS

For ready reference, it is helpful to start with a quick summary of the pertinent features of the system at hand that have been established in earlier work [18, 24]. The observable we focus on is the mean photon number of either field. For definiteness, we consider $\langle N_1 \rangle$. The time series of this observable reveals interesting dynamical features. In the strong nonlinearity regime ($\chi/\lambda \gg 1$), $\langle N_1 \rangle$ undergoes a sequence of bifurcations as κ is varied from 0 to 1. This is depicted in Fig. 1, which corresponds to the values $|\alpha|^2 = 25$ and $\chi/\lambda = 5$. When $\kappa = 0$, $\langle N_1 \rangle$ collapses to a constant value in the time interval $3000 \lesssim \tau \lesssim 9000$, where τ denotes the dimensionless time λt . As κ increases to the value 0.002, this collapse is replaced by a ‘pinched’ effect over the same time interval. Going on, at $\kappa = 0.0033 \equiv \bar{\kappa}$ there is a significantly larger spread in the range of values of $\langle N_1 \rangle$, and the pinch seen for lower values of κ disappears. When κ increases beyond $\bar{\kappa}$, the qualitative behavior of $\langle N_1 \rangle$ reverts to its original form—e.g., the behavior for $\kappa = 0.005$ is very similar to that for $\kappa = 0.002$. Within the computational accuracy involved, $\bar{\kappa} = 0.0033$ is identifiable as a special value of κ (for the given values of $|\alpha|^2$ and χ/λ). With an even further increase in κ , the pinched effect returns in $\langle N_1 \rangle$ sets in. The spacing between successive crests and

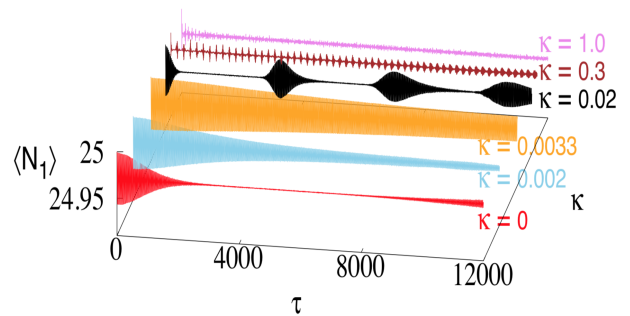


FIG. 1: $\langle N_1 \rangle$ versus time for an initial state $|1; \alpha; \alpha\rangle$, with $|\alpha|^2 = 25$ and $\chi/\lambda = 5$ for different values of κ . (Adapted from Fig. 2 of Ref. [24].)

troughs diminishes with increasing κ . This feature persists up to $\kappa = 1$.

For different values of κ , ϵ -recurrence networks have been constructed [24] from the corresponding time series of $\langle N_1 \rangle$, setting $|\alpha|^2 = 25$ and $\chi/\lambda = 5$. In each case, standard network measures such as the average path length, the link density, the clustering coefficients, the transitivity, the assortativity and the degree distributions have been examined. It has been shown that the clustering coefficient and the transitivity have a maximum value at $\bar{\kappa}$, thus capturing an important feature of the short-time dynamics. We now proceed to investigate the behavior of the MLEs, recurrence plots and first-return-time distributions as a function of κ , with particular reference to the behavior at the special value $\bar{\kappa}$. We also examine whether the clustering coefficient and transitivity maximize at $\bar{\kappa}$ for other choices of the network.

IV. TIME-SERIES ANALYSIS AND NETWORK PROPERTIES

For each given value of κ , a long time series of the mean photon number $\langle N_1 \rangle$ was generated, comprising N_{tot} data points with a scaled time step $\lambda \delta t = 1$. From each of these time series, the first 10000 data points were discarded, to obtain a corresponding time series $\{s(i)\}$ where $1 \leq i \leq N$ and $N = N_{\text{tot}} - 10000$. Hence this set does not include the short-time dynamics—in particular, the bifurcation cascade. The range of values of $\{s(i)\}$ evidently depends on the specific value of κ selected. Next, employing the standard machinery of time-series analysis (see, e.g., [32]), a suitable time delay t_d was identified, and an effective phase space of dimensions $d_{\text{emb}} (\ll N)$ was reconstructed from $\{s(i)\}$. In this space there are $N' = N - (d_{\text{emb}} - 1)t_d$ delay vectors \mathbf{x}_j ($1 \leq j \leq N'$) given by

$$\mathbf{x}_j = [s(j), s(j+t_d), \dots, s(j+(d_{\text{emb}}-1)t_d)]. \quad (6)$$

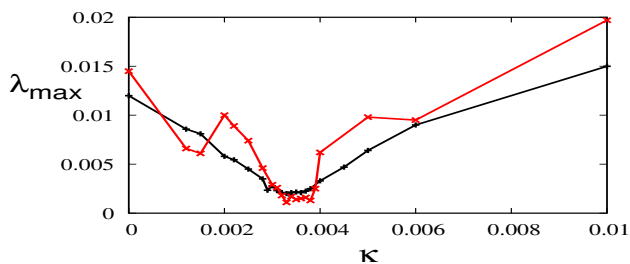


FIG. 2: MLE versus κ for $N = 25000$ (red curve) and $N = 3 \times 10^5$ (black curve). $|\alpha|^2 = 25$ and $\chi/\lambda = 5$. (For interpretation of the colors in the figure(s), the reader is referred to the web version of this article.)

Of the d_{emb} Lyapunov exponents in the phase space, the maximal Lyapunov exponent (MLE) λ_{max} was then computed using the standard TISEAN package [33].

We have compared the manner in which the MLE varies with κ for $N = 25000$ and for $N = 3 \times 10^5$ data points (respectively, the red and black curves in Fig. 2). The two curves are roughly similar, the curve becoming smoother with an increase in N . In particular, we draw

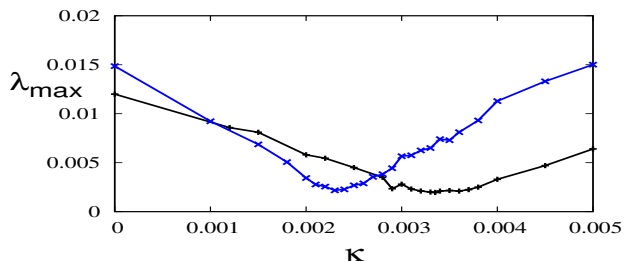


FIG. 3: MLE versus κ with $N = 3 \times 10^5$, $\chi/\lambda = 5$. $|\alpha|^2 = 25$ (black curve) and $|\alpha|^2 = 30$ (blue curve).

attention to the minimum value of the MLE in both cases at $\kappa = \bar{\kappa}$. We have verified that at least 25000 data points are necessary to capture the qualitative behavior of the dynamics in this system. Although the short-time dynamics (including the bifurcation phenomenon around $\bar{\kappa}$) has been excluded in these data sets, the clear minimum in the MLE serves to identify this special value of κ . We note in passing that the reconstructed dynamics is chaotic, but only weakly so, as indicated by the small numerical values of λ_{max} .

For any given value of $|\alpha|^2$, there is a unique special value $\bar{\kappa}$ with the properties described in the foregoing. For instance, when $|\alpha|^2 = 30$, we find that $\bar{\kappa} = 0.0024$ [24]. As before, the MLE has a minimum at $\bar{\kappa}$ (the blue curve in Fig. 3).

We now proceed to examine the return maps, the recurrence plots and the first-return-time distributions for various values of κ with $N = 25000$, $|\alpha|^2 = 25$ and $\chi/\lambda = 5$. From the return maps of $\langle N_1 \rangle$ for different values of κ (Figs. 4(a)-(f)) we can see clear signatures of the special value $\bar{\kappa}$. A prominent annulus appears in the

return map at $\bar{\kappa}$. This feature is absent in the return maps for other values of κ , although other substructures and much smaller annuli are present. As κ approaches 1, these substructures also disappear, and the return maps become more space-filling.

Recurrence plots are standard tools to understand the dynamics in a reconstructed phase space [34–37]. Starting from the $(N' \times N')$ recurrence matrix R with elements

$$R_{ij} = \Theta(\epsilon - \|\mathbf{x}_i - \mathbf{x}_j\|) \quad (7)$$

(where Θ denotes the unit step function and $\|\cdot\|$ is the Euclidean norm), we construct recurrence plots for different values of κ . In doing so, the threshold parameter ϵ must be chosen judiciously. Too small a value of ϵ makes the plot very sparse with very few recurrences, while too large a value yields false recurrences. Several criteria have been proposed in the literature [38–41] for choosing an optimal value of ϵ . We adopt the criterion proposed recently [42] in the context of ϵ -recurrence networks. We consider the $(N' \times N')$ Laplacian matrix L with elements

$$L = D - R + I, \quad (8)$$

where I is the unit matrix, $D = \text{diag}(k_1, \dots, k_{N'})$ and $k_i = \sum_{j=1}^{N'} R_{ij} - 1$. L is a real symmetric matrix, and each of its row sums vanishes. It follows from the structure of L that the eigenvalues of L are real and non-negative, and that at least one of them is zero. Increasing ϵ upward from zero, we determine the smallest value of ϵ (denoted by ϵ_c) for which the next eigenvalue of L becomes nonzero. Recurrence plots ($N' \times N'$ grids with elements R_{ij}) are obtained from Eq.(7) with ϵ set equal to ϵ_c , for various values of κ . These plots highlight the importance of the special value $\bar{\kappa}$ (Figs. 5(a)-(f)). It is evident that the plot is distinctly sparse for $\kappa = \bar{\kappa}$. For other values of κ over the interval $0 \leq \kappa \leq 1$, the corresponding recurrence plots are more dense, some with defined structures and some merely a set of space-filling points.

We turn, next, to the recurrence-time statistics, by first coarse-graining the range of values in the time series of $\langle N_1 \rangle$ for different values of κ into equal-sized cells. The distribution of the time of first return to a generic cell (given that the first time step takes $\langle N_1 \rangle$ to a value outside the initial cell) is obtained. This procedure has been carried out for different initial cells, different cell sizes and for different values of κ . Typical first-return-time distributions are shown in Figs. 6(a)-(f). For values of κ close to 0, the distributions have a single pronounced spike. As κ increases, more spikes appear, and the distributions gradually tend to exponential distributions as $\kappa \rightarrow 1$. For values of κ close to $\bar{\kappa}$ on either side of that value, all the other spikes in the distribution lie to the right of the most pronounced spike. At $\kappa = \bar{\kappa}$, however, all these spikes occur to the left of the most pronounced one. The recurrence-time distribution corresponding to the value $\bar{\kappa}$ is thus distinctly different, qualitatively, from that for all other values of κ .

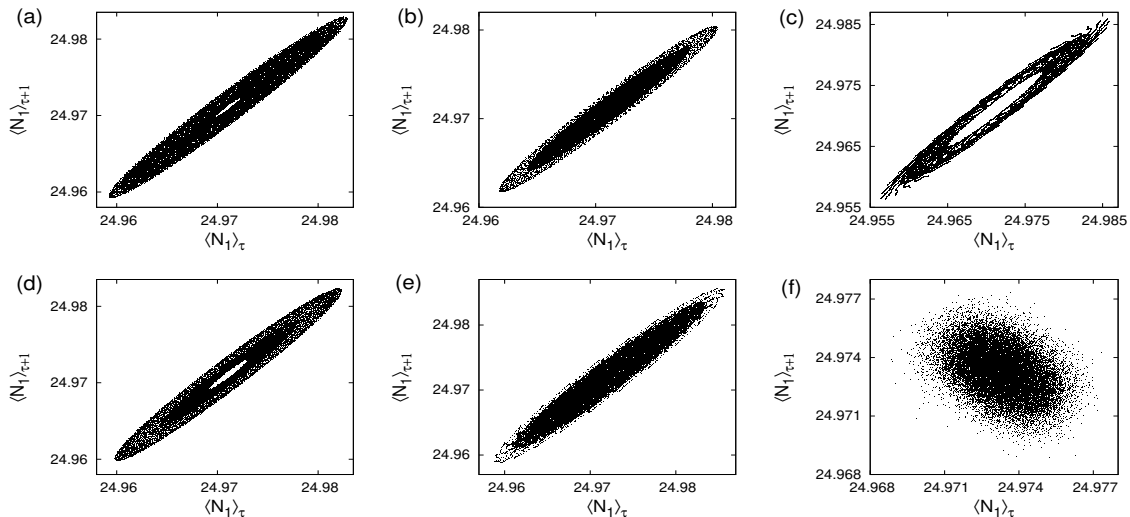


FIG. 4: Return maps of $\langle N_1 \rangle$. $|\alpha|^2 = 25$, $\chi/\lambda = 5$, and $\kappa =$ (a) 0, (b) 0.002, (c) 0.0033, (d) 0.005, (e) 0.02 and (f) 1.

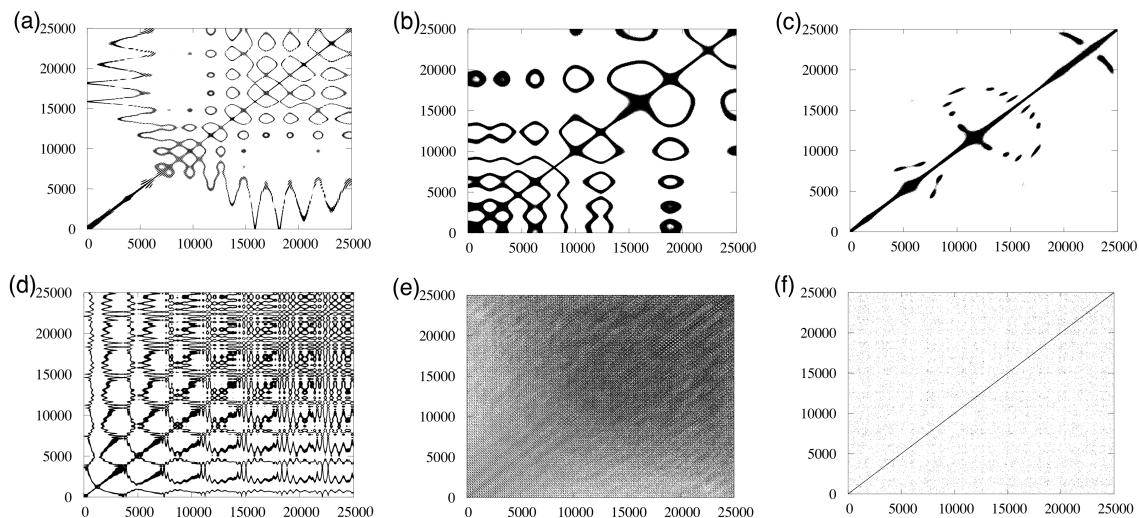


FIG. 5: Recurrence plots of $\langle N_1 \rangle$. $|\alpha|^2 = 25$, $\chi/\lambda = 5$, and $\kappa =$ (a) 0, (b) 0.002, (c) 0.0033, (d) 0.02, (e) 0.3 and (f) 1.

We have verified numerically that the power spectrum is not a good indicator of the special value $\bar{\kappa}$. For completeness however, the corresponding power spectra are shown in Figs. 7(a)-(f).

In [24] we constructed an ϵ -recurrence network from the time series under discussion. In such a network, each vector in the reconstructed phase space is treated as a node of a network, and two nodes are connected if the distance between them is less than the value ϵ_c defined in the foregoing. Among other measures we considered the link density (LD), the clustering coefficient (CC) and the transitivity (\mathcal{T}) [8, 43, 44] of the network. For ready reference we quote the definitions of these quantities. The

link density LD of a network of N' nodes is defined as

$$\text{LD} = [N'(N' - 1)]^{-1} \sum_i k_i, \quad (9)$$

where $k_i = \sum_{j=1}^{N'} A_{ij}$ is now the degree of the node i in terms of the elements $A_{ij} = R_{ij} - \delta_{ij}$ of the adjacency matrix A . The local clustering coefficient, which measures the probability that two randomly chosen neighbours of a given node i are directly connected, is defined as

$$C_i = [k_i(k_i - 1)]^{-1} \sum_{j,k} A_{jk} A_{ij} A_{ik}. \quad (10)$$

The global clustering coefficient CC is the arithmetic mean of the local clustering coefficients taken over all the

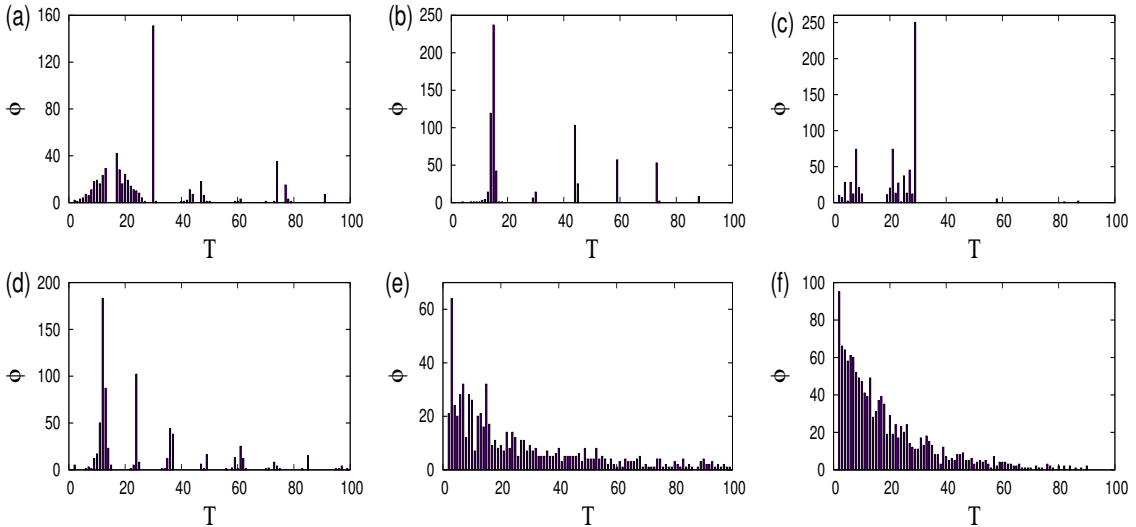


FIG. 6: First-return-time distribution of $\langle N_1 \rangle$ for 50 equal-sized cells. $|\alpha|^2 = 25$, $\chi/\lambda = 5$, and $\kappa =$ (a) 0, (b) 0.002, (c) 0.0033, (d) 0.02, (e) 0.3 and (f) 1.

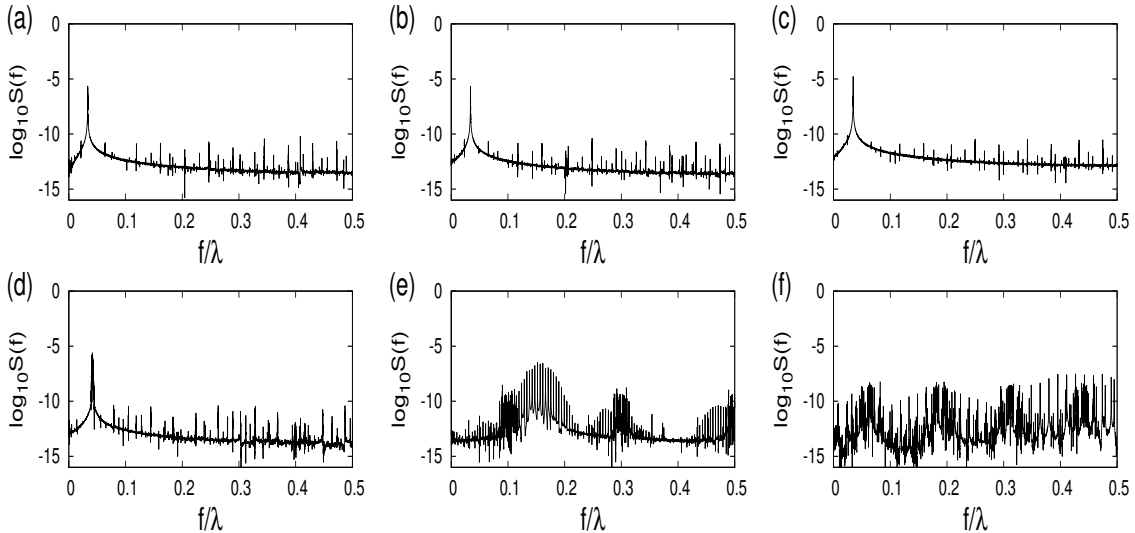


FIG. 7: Power spectrum of $\langle N_1 \rangle$. $|\alpha|^2 = 25$, $\chi/\lambda = 5$, $\kappa =$ (a) 0, (b) 0.002, (c) 0.0033, (d) 0.02, (e) 0.3 and (c) 1.

nodes of the network. The transitivity \mathcal{T} of the network is defined as

$$\mathcal{T} = \frac{\sum_{i,j,k}^{N'} A_{ij} A_{jk} A_{ki}}{\sum_{i,j,k}^{N'} A_{ij} A_{ki}}. \quad (11)$$

For the effective time series with $N = 25000$, it was shown that the CC and \mathcal{T} attain a maximum at $\kappa = \bar{\kappa}$ (see, e.g., Fig. 6 of Ref. [24]). We now establish that, even with a very different and considerably simpler procedure for choosing ϵ_c , the CC and \mathcal{T} enable us to single out the special value $\bar{\kappa}$: the threshold ϵ_c is just the value of ϵ for which the link density has an optimal value. (It has been suggested [8] that this value of the LD should be below 0.05.) We find that in this procedure of choosing an ϵ_c , too, both the CC and \mathcal{T} are maximum at $\kappa = \bar{\kappa}$

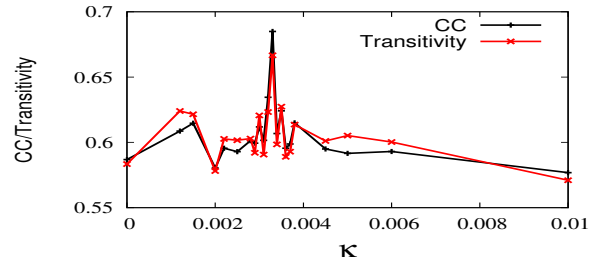


FIG. 8: ϵ -recurrence network: clustering coefficient and transitivity versus κ for $|\alpha|^2 = 25$ and $\chi/\lambda = 5$.

(Fig. 8). This conclusion is supported by extensive numerical results for a range of values of $|\alpha|^2$ and LD. We

conclude that an ϵ -recurrence network and the straightforward calculation of its CC and \mathcal{T} provide the simplest means of identifying the special value of the bifurcation parameter κ in the model under study.

V. CONCLUDING REMARKS

We have investigated, using the machinery of nonlinear time-series analysis, the dynamics of a tripartite quantum system comprising a Λ -atom interacting with two initially coherent radiation fields with inherent nonlinearities and an intensity-dependent field-atom coupling (IDC). In earlier work, the short-time dynamics of the mean photon number $\langle N_1 \rangle$ was shown to display a sequence of bifurcations as a function of the IDC parameter κ , in which $\langle N_1 \rangle$ shifts from collapse to a constant value to oscillatory behavior. A special value $\bar{\kappa}$ of the parameter separates the two kinds of behavior. An ϵ -recurrence network constructed from the time series showed that the clustering coefficient and the transitivity also displayed signatures of this special value $\bar{\kappa}$.

In this Letter, we have examined several other relevant aspects of the time series, including the maximum Lyapunov exponents, the return maps, the recurrence plots and the first-return-time distributions. We have established that the existence of the special value $\bar{\kappa}$ is mirrored in each of these quantities, and the corresponding distinguishing feature has been identified in each case. We have further shown that, independent of the details of the network considered, the clustering coefficient and transitivity carry distinct and easily identifiable signatures of $\bar{\kappa}$.

The novelty and importance of this investigation lie in the interesting link established between short-time bifurcation phenomena, on the one hand, and on the other, network parameters, indicators from dynamical systems theory such as the qualitative features of recurrences, and quantifiers such as the maximal Lyapunov exponent. The model we have studied is a generic one, and the results suggest that the inferences drawn in this case could be generalized to a wide class of quantum systems. More detailed investigations in this regard would be a useful direction of future research, particularly for understanding possible links between group-theoretic structures on the one hand and the dynamics of quantum observables over short and long time scales on the other.

Nonlinear quantum optics experiments, i.e., attempts to realize photon-photon interactions through *nonlinear coupling of photons to an atom* have gained tremendous importance in recent years (see, e.g., [45]). The primary motivation is the belief that, in this regime of quantum optics, the performance of devices made for quantum technologies and quantum information processing would be far superior to that of devices based on classical optics, linear quantum optics, and even nonlinear optics with weak atom-photon coupling. The main challenge lies in achieving strong nonlinear interactions even with low in-

tensity light. The fact that this target can be achieved through specific kinds of atom-photon coupling is what validates the model we have used, from the point of view of potential experiments. The coupling should clearly be tunable to take into account different levels of light intensity in experiments: in our model, the parameter κ multiplies the photon number operator (or intensity). Further, it is known that a model comprising a *two*-level atom interacting with a photon through appropriate couplings has limitations, in the sense that the electronic states of the atom have short lifetimes which prevents them from retaining ‘memory’ of their interactions with the photon over longer time intervals. This makes it necessary for at least two photons to arrive simultaneously at the atom, but that leads to spatial entanglement between the two photons which complicates the results. Hence, a three-level or multi-level atom with two radiation fields which mediate two different transitions is recognized by experimenters as the set-up required. The simplest of course would be the ‘workhorse’, namely the Λ atom interacting with two fields, which is the model we have employed.

In this Letter we have explored the complexity of quantum dynamics in a model which is a *paradigm* of the general features and possibilities we seek to investigate and categorize. Now, a detailed body of knowledge has been built up regarding complex behavior in *classical* dynamical systems with the help of representative models, in particular, low-dimensional maps and flows. The latter are caricatures of real physical systems, and are not in general faithful representations of actual experimental situations. Nevertheless, their detailed analysis yields very valuable information on the essential and salient features of the dynamics they are intended to demonstrate. A similar objective validates the kind of theoretical analysis we have reported here on paradigmatic quantum mechanical systems.

Appendix A: The state vector

The Hamiltonian defined in Eq.(2) can be written as the sum $H_0 + H_1$, where $H_0 = \sum_{i=1}^2 \Omega_i N_i^{\text{tot}} + \omega_3 I$ (merely introduces a phase factor in the time evolved state), and

$$H_1 = \sum_{i=1}^2 \left[\chi a_i^\dagger a_i^2 - \Delta_i \sigma_{ii} + \lambda \{ a_i f(N_i) \sigma_{3i} + f(N_i) a_i^\dagger \sigma_{i3} \} \right]. \quad (\text{A1})$$

Here $I = \sum_{j=1}^3 \sigma_{jj}$, $N_i^{\text{tot}} = a_i^\dagger a_i - \sigma_{ii}$ ($i = 1, 2$) are constants of the motion, and the two detuning parameters $\Delta_i = \omega_3 - \omega_i - \Omega_i$. For convenience, we set $\Delta_i = 0$.

The coefficients $A_{nm}(t)$, $B_{nm}(t)$, and $C_{nm}(t)$ in Eq.(5)

satisfy the following coupled equations

$$\dot{A}_{nm}(t) = (V_{11} + V_{22})A_{nm}(t) + f_1 C_{nm}(t), \quad (\text{A2})$$

$$\dot{B}_{nm}(t) = (V_{12} + V_{21})B_{nm}(t) + f_2 C_{nm}(t), \quad (\text{A3})$$

$$\dot{C}_{nm}(t) = (V_{12} + V_{21})C_{nm}(t) + f_1 A_{nm}(t) + f_2 B_{nm}(t), \quad (\text{A4})$$

with

$$V_{11} = \chi n(n-1), \quad V_{12} = \chi(n-1)(n-2), \quad (\text{A5})$$

$$V_{21} = \chi m(m+1), \quad V_{22} = \chi m(m-1), \quad (\text{A6})$$

$$f_1 = \lambda n^{1/2} f(n), \quad f_2 = \lambda(m+1)^{1/2} f(m+1). \quad (\text{A7})$$

Since the atom is initially in $|1\rangle$, it cannot make a transition to $|3\rangle$ if $n = 0$. Hence $A_{0m}(t) = 1$, $B_{0m}(t) = C_{0m}(t) = 0$ for all m . When $n, m \geq 1$, we find

$$A_{nm}(t) = \frac{1}{f_1 f_2} \sum_{j=1}^3 \left[(\mu_j + V_{12} + V_{22})(\mu_j + V_{12} + V_{21}) - f_2^2 \right] b_j e^{i\mu_j t}, \quad (\text{A8a})$$

$$B_{nm}(t) = \sum_{j=1}^3 b_j e^{i\mu_j t}, \quad (\text{A8b})$$

$$C_{nm}(t) = -\frac{1}{f_2} \sum_{j=1}^3 (\mu_j + V_{12} + V_{21}) b_j e^{i\mu_j t}. \quad (\text{A8c})$$

Here, f_1 and f_2 capture the effect of $f(N)$ in the Hamiltonian on the state of the system. Further, for $j = 1, 2, 3$,

$$\mu_j = -\frac{1}{3} x_1 + \frac{2}{3} (x_1^2 - 3x_2)^{1/2} \cos \left\{ \theta + \frac{2}{3}(j-1)\pi \right\}, \quad (\text{A9})$$

and

$$\theta = \frac{1}{3} \cos^{-1} \left\{ [9x_1 x_2 - 2x_1^3 - 27x_3] / [2(x_1^2 - 3x_2)^{3/2}] \right\}, \quad (\text{A10})$$

with

$$x_1 = V_{11} + 2V_{12} + V_{21} + 2V_{22}, \quad (\text{A11})$$

$$x_2 = (V_{12} + V_{21})(V_{11} + V_{12} + 2V_{22}) + (V_{12} + V_{22})(V_{11} + V_{22}) - f_1^2 - f_2^2, \quad (\text{A12})$$

$$x_3 = (V_{12} + V_{21}) [(V_{12} + V_{22})(V_{11} + V_{22}) - f_1^2] - f_2^2 (V_{11} + V_{22}), \quad (\text{A13})$$

and

$$b_j = f_1 f_2 / [(\mu_j - \mu_k)(\mu_j - \mu_l)], \quad j \neq k \neq l. \quad (\text{A14})$$

Finally, for $m = 0$, we find $B_{n0}(t) = 0$ and

$$A_{n0}(t) = \sum_{j=1}^2 c_j e^{i\alpha_j t}, \quad (\text{A15})$$

$$C_{n0}(t) = -\frac{1}{f_1} \sum_{j=1}^2 c_j (\alpha_j + V_{11}) e^{i\alpha_j t}. \quad (\text{A16})$$

Here

$$c_1 = \frac{V_{11} + \alpha_2}{\alpha_2 - \alpha_1}, \quad c_2 = \frac{V_{11} + \alpha_1}{\alpha_1 - \alpha_2}, \quad (\text{A17})$$

and

$$\alpha_1 = \frac{1}{2} [-y_1 + (y_1^2 - 4y_2)^{1/2}], \quad (\text{A18})$$

$$\alpha_2 = \frac{1}{2} [-y_1 - (y_1^2 - 4y_2)^{1/2}], \quad (\text{A19})$$

where

$$y_1 = V_{11} + V_{12}, \quad y_2 = V_{12} V_{11} - f_1^2. \quad (\text{A20})$$

Denoting by $\rho_1(t)$ and $\rho_2(t)$, the reduced density matrices for the fields F_1 and F_2 respectively, we get (after dropping the explicit time dependence from each of the coefficients)

$$\langle n | \rho_1(t) | n' \rangle = \sum_{l=0}^{\infty} q_n q_{n'}^* |r_l|^2 A_{n,l} A_{n',l}^* + \sum_{l=1}^{\infty} q_{n+1} q_{n'+1}^* |r_{l-1}|^2 B_{n+1,l-1} B_{n'+1,l-1}^* + \sum_{l=0}^{\infty} q_{n+1} q_{n'+1}^* |r_l|^2 C_{n+1,l} C_{n'+1,l}^*, \quad (\text{A21})$$

$$\langle l | \rho_2(t) | l' \rangle = \sum_{n=0}^{\infty} \left[|q_n|^2 r_l r_{l'}^* A_{n,l} A_{n,l'}^* + (1 - \delta_{l,0})(1 - \delta_{l',0}) (|q_{n+1}|^2 r_{l-1} r_{l'-1}^* B_{n+1,l-1} B_{n+1,l'-1}^*) + |q_{n+1}|^2 r_l r_{l'}^* C_{n+1,l} C_{n+1,l'}^* \right]. \quad (\text{A22})$$

[1] S. Lloyd, S. Garnerone, and P. Zanardi, Nat. Commun. **7**, 1 (2016).

[2] P. Reberntrost, M. Mohseni, and S. Lloyd, Phys. Rev.

Lett. **113**, 130503 (2014).

[3] Y. Zou, R. V. Donner, J. F. Donges, N. Marwan, and J. Kurths, Chaos **20**, 043130 (2010).

- [4] Z. Gao and N. Jin, *Phys. Rev. E* **79**, 066303 (2009).
- [5] J. F. Donges, R. V. Donner, K. Rehfeld, N. Marwan, M. H. Trauth, and J. Kurths, *Nonlin. Processes Geophys.* **18**, 545 (2011).
- [6] N. Marwan, N. Wessel, U. Meyerfeldt, A. Schirdewan, and J. Kurths, *Phys. Rev. E* **66**, 026702 (2002).
- [7] G. M. Ramírez Ávila, A. Gapelyuk, N. Marwan, T. Walther, H. Stepan, J. Kurths, and N. Wessel, *Philos. Trans. R. Soc. London A* **371** (2013).
- [8] Y. Zou, R. V. Donner, N. Marwan, J. F. Donges, and J. Kurths, *Phys. Rep.* **787**, 1 (2019).
- [9] P. Wittek, *Quantum Machine Learning* (Elsevier, London, 2014).
- [10] G. S. Agarwal and R. R. Puri, *Phys. Rev. A* **39**, 2969 (1989).
- [11] C. Sudheesh, S. Lakshmibala, and V. Balakrishnan, *Phys. Lett. A* **373**, 2814 (2009).
- [12] C. Sudheesh, S. Lakshmibala, and V. Balakrishnan, *Europhys. Lett.* **90**, 50001 (2010).
- [13] A. Shankar, S. Lakshmibala, and V. Balakrishnan, *J. Phys. B: At. Mol. Opt. Phys.* **47**, 215505 (2014).
- [14] P. Laha, S. Lakshmibala, and V. Balakrishnan, *J. Mod. Opt.* **65**, 1466 (2018).
- [15] P. Laha, S. Lakshmibala, and V. Balakrishnan, *J. Opt. Soc. Am. B* **36**, 575 (2019).
- [16] B. Sharmila, K. Saumitran, S. Lakshmibala, and V. Balakrishnan, *J. Phys. B: At. Mol. Opt. Phys.* **50**, 045501 (2017).
- [17] T. Yu and J. H. Eberly, *Science* **323**, 598 (2009).
- [18] P. Laha, B. Sudarsan, S. Lakshmibala, and V. Balakrishnan, *Int. J. Th. Phys.* **55**, 4044 (2016).
- [19] Y.-S. Chin, M. Steiner, and C. Kurtsiefer, *Nat. Commun.* **8**, 1200 (2017).
- [20] B. Buck and C. Sukumar, *Phys. Lett. A* **81**, 132 (1981).
- [21] E. C. G. Sudarshan, *Int. J. Th. Phys.* **32**, 1069 (1993).
- [22] S. Sivakumar, *J. Phys. A: Math. Gen.*, **35**, 6755 (2002).
- [23] S. Barzanjeh, M. H. Naderi, and M. Soltanolkotabi, *Phys. Rev. A* **84**, 023803 (2011).
- [24] P. Laha, S. Lakshmibala, and V. Balakrishnan, *Europhys. Lett.* **125**, 60005 (2019).
- [25] Y.-q. Li and M. Xiao, *Phys. Rev. A* **51**, R2703 (1995).
- [26] M. Fleischhauer, A. Imamoglu, and J. P. Marangos, *Rev. Mod. Phys.* **77**, 633 (2005).
- [27] X. Yang, J. Sheng, U. Khadka, and M. Xiao, *Phys. Rev. A* **85**, 013824 (2012).
- [28] X. Yang and M. Xiao, *Sci. Rep.* **5**, 13609 (2015).
- [29] G. R. Honarasa and M. K. Tavassoly, *Phys. Scr.* **86**, 035401 (2012).
- [30] E. Ghasemian and M. K. Tavassoly, *J. Opt. Soc. Am. B* **35**, 86 (2018).
- [31] H. Wang, D. Goorskey, and M. Xiao, *Phys. Rev. Lett.* **87**, 073601 (2001).
- [32] H. D. Abarbanel, *Analysis of Observed Chaotic Data* (Springer, Berlin, 1996).
- [33] R. Hegger, H. Kantz, and T. Schreiber, *Chaos* **9**, 413 (1999).
- [34] J.-P. Eckmann, S. O. Kamphorst, and D. Ruelle, *Europhys. Lett.* **4**, 973 (1987).
- [35] M. Thiel, M. C. Romano, and J. Kurths, *Phys. Lett. A* **330**, 343 (2004).
- [36] N. Marwan, M. C. Romano, M. Thiel, and J. Kurths, *Phys. Rep.* **438**, 237 (2007).
- [37] N. Marwan, *Eur. Phys. J. Spec. Top.* **164**, 3 (2008).
- [38] G. M. Mindlin and R. Gilmore, *Physica D* **58**, 229 (1992).
- [39] J. P. Zbilut and C. L. Webber, *Phys. Lett. A* **171**, 199 (1992).
- [40] J. P. Zbilut, J.-M. Zaldívar-Comenges, and F. Strozzi, *Phys. Lett. A* **297**, 173 (2002).
- [41] M. Thiel, M. Romano, J. Kurths, R. Meucci, E. Allaria, and F. Arecchi, *Physica D* **171**, 138 (2002).
- [42] D. Eroglu, N. Marwan, S. Prasad, and J. Kurths, *Nonlin. Processes Geophys.* **21**, 1085 (2014).
- [43] S. Boccaletti, V. Latora, Y. Moreno, M. Chavez, and D.-U. Hwang, *Phys. Rep.* **424**, 175 (2006).
- [44] D. J. Watts and S. H. Strogatz, *Nature* **393**, 440 (1998).
- [45] D. Chang, V. Vuletic, and M. Lukin, *Nature Photonics* **8**, 685 (2014).